

## Article

# Development of Au Nanoparticle Two-Dimensional Assemblies Dispersed with Au Nanoparticle-Nanostar Complexes and Surface-Enhanced Raman Scattering Activity

Kosuke Sugawa <sup>1,\*</sup> , Kaichi Ono <sup>1</sup>, Ritsurai Tomii <sup>1</sup>, Yuka Hori <sup>1</sup>, Yu Aoki <sup>1</sup>, Koki Honma <sup>1</sup>, Kaoru Tamada <sup>2</sup>  and Joe Otsuki <sup>1</sup> 

<sup>1</sup> Department of Materials and Applied Chemistry, College of Science and Technology, Nihon University, Kanda-Surugadai, Chiyoda-ku, Tokyo 101-8308, Japan

<sup>2</sup> Institute for Materials Chemistry and Engineering (IMCE), Kyushu University, 744 Motooka, Nishiku, Fukuoka 819-0395, Japan

\* Correspondence: sugawa.kosuke@nihon-u.ac.jp

**Abstract:** We recently found that polyvinylpyrrolidone (PVP)-protected metal nanoparticles dispersed in water/butanol mixture spontaneously float to the air/water interface and form two-dimensional assemblies due to classical surface excess theory and Rayleigh–Bénard–Marangoni convection induced by butanol evaporation. In this study, we found that by leveraging this principle, a unique structure is formed where hetero gold nanospheres (AuNPs)/gold nanostars (AuNSs) complexes are dispersed within AuNP two-dimensional assemblies, obtained from a mixture of polyvinylpyrrolidone-protected AuNPs and AuNSs that interact electrostatically with the AuNPs. These structures were believed to form as a result of AuNPs/AuNSs complexes formed in the water/butanol mixture floating to the air/water interface and being incorporated into the growth of AuNP two-dimensional assemblies. These structures were obtained by optimizing the amount of mixed AuNSs, with excessive addition resulting in the formation of random three-dimensional network structures. The AuNP assemblies dispersed with AuNPs/AuNSs complexes exhibited significantly higher Raman (surface-enhanced resonance Raman scattering: SERRS) activity compared to simple AuNP assemblies, while the three-dimensional network structure did not show significant SERRS activity enhancement. These results demonstrate the excellent SERRS activity of AuNP two-dimensional assemblies dispersed with hetero AuNPs/AuNSs complexes.

**Keywords:** surface-enhanced resonance Raman scattering; two-dimensional assemblies; Au nanostars; self-assembly; heterostructures; localized surface plasmon resonance



**Citation:** Sugawa, K.; Ono, K.; Tomii, R.; Hori, Y.; Aoki, Y.; Honma, K.; Tamada, K.; Otsuki, J. Development of Au Nanoparticle Two-Dimensional Assemblies Dispersed with Au Nanoparticle-Nanostar Complexes and Surface-Enhanced Raman Scattering Activity. *Nanomaterials* **2024**, *14*, 764. <https://doi.org/10.3390/nano14090764>

Academic Editor: Vlad Stolojan

Received: 28 March 2024

Revised: 19 April 2024

Accepted: 23 April 2024

Published: 26 April 2024



**Copyright:** © 2024 by the authors. Licensee MDPI, Basel, Switzerland. This article is an open access article distributed under the terms and conditions of the Creative Commons Attribution (CC BY) license (<https://creativecommons.org/licenses/by/4.0/>).

## 1. Introduction

Surface-enhanced Raman scattering (SERS) is a highly sensitive molecular fingerprinting technique with applications expected in fields such as diagnostics and biomedical imaging [1,2]. When functional molecules are in close proximity to noble metal nanoparticles, their Raman signals can be significantly enhanced depending on the strong electromagnetic fields generated upon excitation of localized surface plasmon (LSP) resonance of the nanoparticles [3–5]. The high-density assembly of noble metal nanoparticles has been recognized as a valuable means to control the properties of local electromagnetic fields. This is because the proximity of multiple plasmonic metal nanoparticles within such assemblies can induce plasmon coupling, potentially generating significantly concentrated electromagnetic fields, known as hotspots, within the nanogap spaces between the particles [6–10]. Therefore, the development of techniques to further control these plasmon coupling properties has led to the development of platforms with even higher SERS activity [11,12].

Typically, the plasmon coupling has been induced by the proximity of identical nanoparticles [6]. In addition, one approach that has recently gained attention for controlling the properties of plasmon coupling is the utilization of the coupling between LSPR resonances of metal nanoparticles of different shapes [13–15], sizes [16,17], and materials [18–20]. In studies modeling heterodimers composed of spherical gold nanoparticles (AuNPs) and gold nanocubes, variations in the dimer morphology have been reported to result in variations in the plasmon coupling properties, such as resonance wavelength [13] and electromagnetic field intensity [14,21]. Furthermore, gold nanostars (AuNSs), which possess a star-shaped structure, not only induce significant local electromagnetic fields through their LSP resonance [22,23] but also have the potential to exhibit even stronger fields when coupled with the LSP resonance of AuNPs in the AuNPs/AuNSs complexes [24,25]. On the other hand, many of the morphologies used in these studies involve heterodimer structures where two nanoparticles are brought into close proximity [13,14], or core-satellite structures [26]. These structures are suitable for studying the fundamental properties of plasmon coupling, but their application as SERS platforms that utilize the strong electromagnetic field spaces is challenging. Therefore, research focusing on utilizing this distinctive plasmon coupling in high-density two-dimensional assemblies of metal nanoparticles, which have demonstrated utility as SERS sensing platforms [27–29], has recently attracted particular attention [30,31]. For example, the SERS activity of two-dimensional assemblies composed of two components, AuNPs and Au@Ag nanocubes, has been reported to be significantly stronger compared to the two-dimensional assemblies consisting of single-component Au nanoparticles or Au@Ag nanocubes alone, attributed to strong plasmon coupling in heterodimers [30]. However, such studies remain rare, and the development of two-dimensional assemblies of metal nanoparticles exhibiting the aforementioned distinctive plasmon coupling properties could be a significant approach towards further SERS-active platforms.

Two-dimensional assemblies of metal nanoparticles have frequently been developed using bottom-up approaches, which offer advantages in terms of cost and simplicity. Many of these techniques utilize the interactions between metal nanoparticles, as well as between nanoparticles and the interface induced by the evaporation of dispersed solvents [32,33] and surface modifiers (or promoters) [34,35], to assemble metal nanoparticles at air/liquid or liquid/liquid interfaces. In addition, we have recently established a method for developing two-dimensional assemblies from metal nanoparticles dispersed in a mixed solution of short-chain alcohol (butanol) and water, based on classical surface excess theory and Rayleigh–Bénard–Marangoni convection induced by the vaporization of butanol [36]. The characteristic of this method is that metal nanoparticles protected by polyvinylpyrrolidone (PVP) interact strongly with butanol in the mixed solution, are induced to the air–liquid interface through microscopic convection, and then assembled. In this study, we observed the spontaneous formation of unique structures, where AuNPs/AuNSs complexes were sparsely dispersed within AuNP assemblies (AuNP/AuNS-in-assemblies), from a water/BuOH solution containing PVP-protected AuNPs and AuNSs interacting electrostatically with them. Here, “AuNPs/AuNSs complexes” refer to composite structures formed from AuNSs and AuNPs through electrostatic interactions between them. Furthermore, notably, the SERS activity of these assemblies was higher compared to simple two-dimensional assemblies of AuNPs. These results suggest that the developed assemblies function as high-performance SERS sensing platforms incorporating the characteristic plasmon coupling between AuNSs and AuNPs.

## 2. Materials and Methods

### 2.1. Materials

In this study, Milli-Q water (18.2 M $\Omega$ ) was used to prepare all aqueous solutions. Chloroauric(III) acid tetrahydrate (HAuCl<sub>4</sub>, Nacalai Tesque, Kyoto, Japan), trisodium citrate dihydrate (Kanto Chemical, Tokyo, Japan), hydrochloric acid (Kishida Chemical, Osaka, Japan), silver nitrate (Fujifilm Wako Pure Chemical, Osaka, Japan), L-ascorbic acid

(Tokyo Chemical Industry, Tokyo, Japan), 1-butanol (BuOH, Kishida Chemical), ethanol (Kishida Chemical), sodium hydroxide (Kanto Chemical), 16-mercaptohexadecanoic acid (MHA, Sigma-Aldrich, St. Louis, MO, USA), polyethyleneimine (PEI, MW: ~10,000, Fujifilm Wako Pure Chemical) and PVP (MW: ~55,000, Sigma-Aldrich, Saint Louis, MO, USA) were used without further purification.

## 2.2. Synthesis of AuNPs and AuNSs

The synthesis of AuNPs was achieved by reducing  $\text{HAuCl}_4$  with citric acid [37]. Specifically, AuNPs were synthesized by refluxing a 0.01 wt.%  $\text{HAuCl}_4$  aqueous solution at 100 °C for 30 min, followed by the addition of a 1 wt.% aqueous solution of trisodium citrate (0.9 mL) and continuing the reflux for an additional 1 h. AuNSs were synthesized using a modified seed-mediated method [38]. The gold nanoparticle seeds were synthesized using the citrate reduction method mentioned above. The volume of a 1 wt.% trisodium citrate solution added to the  $\text{HAuCl}_4$  aqueous solution was adjusted to 4 mL to synthesize the gold nanoparticle seeds with a diameter of 12 nm. A 1 mL colloidal aqueous solution of gold nanoparticle seeds was mixed with 100 mL of 0.01 wt.%  $\text{HAuCl}_4$  aqueous solution, 700  $\mu\text{L}$  of 1 mM hydrochloric acid, and 1 mL of 2 mM silver nitrate. Upon addition of 500  $\mu\text{L}$  of an aqueous solution containing 0.1 M L-ascorbic acid to this mixed solution, AuNSs were synthesized. To prevent aggregation of the AuNSs, 0.7 mL of a 1 wt.% trisodium citrate aqueous solution and 3 mL of a 1 M sodium hydroxide aqueous solution were added, followed by stirring the mixture for approximately 10 min.

## 2.3. Surface Modification of AuNPs and AuNSs

The surface of citrate-modified AuNPs was sequentially modified with MHA, PEI, and PVP. A 5 mM MHA ethanol solution (0.9 mL) was added to the colloidal AuNPs solution (15 mL) under stirring, followed by stirring for approximately 15 min to immobilize MHA on the AuNPs surface. The resulting colloidal solution underwent purification through centrifugation (5600 rpm, 5 min). The resulting precipitate was dispersed in 5 mL of ethanol and added to a 15 mL ethanol solution of 4 mg/mL PEI, followed by stirring for 15 min to electrostatically immobilize PEI onto the MHA-modified AuNPs. This solution was also purified by centrifugation (6500 rpm, 10 min) and dispersed in 5 mL of ethanol. The colloidal solution was then added to a 0.7 mM ethanol solution of PVP (15 mL) and stirred for approximately 15 min to modify the outermost surface of the AuNPs with PVP [36]. This mixed solution underwent centrifugation twice (7000 rpm, 10 min) and was finally dispersed in BuOH (0.12 mL). The surface of AuNSs was modified with MHA utilizing the same method as the MHA modification on the surface of AuNPs.

## 2.4. Self-Assembly of Au Nanoparticles at the Air/Water Interface

A solution of BuOH (0.12 mL) containing  $5.5 \times 10^{11}$  AuNPs with PVP-modified surfaces was mixed with an aqueous solution (2.4 mL) containing  $5.3 \times 10^8$ ,  $1.1 \times 10^9$ ,  $2.1 \times 10^9$ ,  $3.2 \times 10^9$ , or  $4.3 \times 10^9$  AuNSs with MHA-modified surfaces in a sample vial and stirred for 10 s. Afterwards, the mixed solution was quickly transferred to a petri dish with a diameter of 2.8 cm and left to stand. For all samples, a liquid-like film of nanoparticles formed at the air/water interface within 90 min. The nanoparticle assemblies, which were transferred on the surface of glass plate, were treated with low-pressure plasma (intensity: 10, time: 90 s).

## 2.5. Measurements

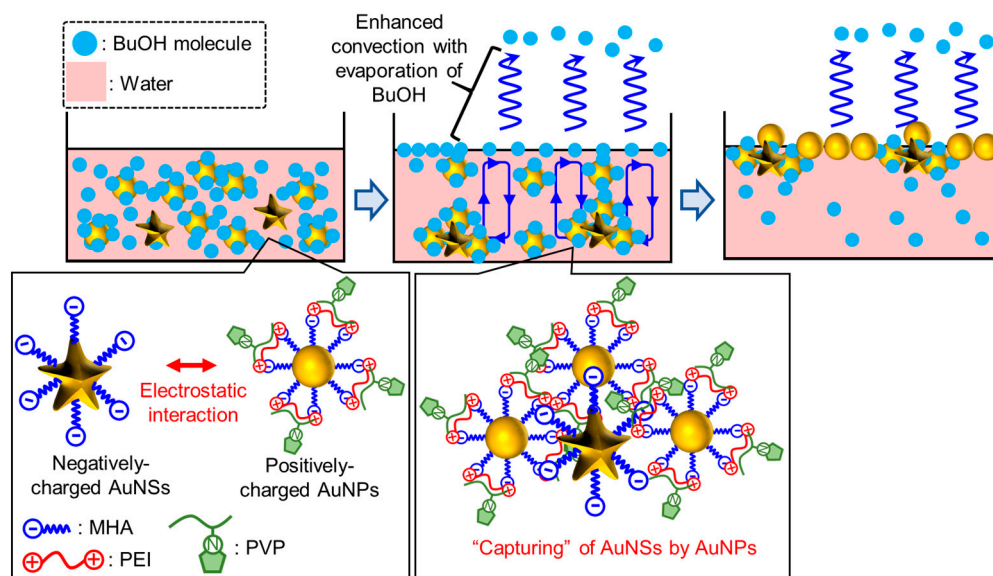
UV-visible near-infrared spectroscopy was performed using a JASCO V-770 spectrophotometer (Tokyo, Japan). Field-emission scanning electron microscopy (FE-SEM) images were taken using a Hitachi S-4500. (Tokyo, Japan) Transmission electron microscopy (TEM) images were taken using a Hitachi HF-2000 (Tokyo, Japan). Atomic force microscopy (AFM) measurements were performed with a Hitachi SPI-3800N-SPA400 (Tokyo, Japan). The Raman scattering spectra were measured using a micro-Raman spectrometer (JASCO

NRS-4100, Tokyo, Japan). A 785 nm continuous-wave (CW) laser (Sun Instruments, Tokyo, Japan) was used as the excitation light source. The modification of the probe molecule, indocyanine green (ICG), onto the sample substrate was achieved by casting a 50  $\mu\text{L}$  solution of  $1 \times 10^{-6}$  M ICG onto the sample substrate and allowing it to dry. The laser was directed onto the sample surface through a  $20\times$  working distance objective lens. Dynamic light scattering measurements were performed using a Zetasizer Nano ZS (Malvern Panalytical, Great Malvern, UK).

### 3. Results

#### 3.1. Construction of AuNPs/AuNSs Complex-Dispersed AuNP Two-Dimensional Assemblies

In this study, the estimated formation mechanism of AuNP/AuNS-in-assemblies is illustrated in Scheme 1. The AuNSs are assumed to be modified with MHA, while the AuNPs are assumed to be sequentially modified with MHA, PEI, and PVP. As a result, the surface of AuNSs is expected to carry a negative charge, while that of AuNPs is expected to be positively charged, reflecting the charges of the modified molecules. Furthermore, we have previously confirmed that only the metal nanoparticles protected by PVP, which strongly interact with BuOH, assemble at the air/water interface using the assembly method we developed in the past [36]. Therefore, AuNSs dispersed in water/BuOH are not expected to spontaneously assemble at the air/water interface. On the other hand, the coexistence of AuNPs and AuNSs in a water/BuOH solution is expected to lead to the formation of complexes between them through electrostatic attraction within the solution. As a result, AuNPs/AuNSs complexes, composed of AuNPs capable of assembling at the air/water interface, are expected to accumulate at the interface. On the other hand, if the number of AuNPs significantly exceeds that of AuNSs, it is anticipated that AuNPs, which do not form complexes with AuNSs, will independently assemble at the air/water interface, resulting in the formation of high-density two-dimensional assemblies. Consequently, the formation of AuNP/AuNS-in-assemblies is anticipated.



**Scheme 1.** Scheme for the fabrication of AuNP/AuNS-in-assemblies.

In the experiments, AuNPs with an average diameter of  $53 \pm 5$  nm and AuNSs with sizes ranging approximately from 130 to 200 nm were used (TEM image: Figure S1). As anticipated, zeta potential measurements revealed surface charges of  $-42.4$  mV for AuNSs modified with MHA and  $8.16$  mV for AuNPs modified with MHA-PEI-PVP. These nanoparticles were dispersed in a water/BuOH solution. The number of AuNPs in the solution was fixed at  $5.5 \times 10^{11}$ , while the number of AuNSs was varied in five increments ranging from  $5.3 \times 10^8$  to  $4.3 \times 10^9$ .

First, to verify the formation of AuNPs/AuNSs complexes in water/BuOH, the extinction spectrum of the colloidal solution immediately after mixing both nanoparticles in the solution was measured (Figure 1A). Under conditions where the number of AuNSs was high ( $>1.1 \times 10^9$ ), a distinct LSP resonance band of AuNSs was observed in the near-infrared region, in addition to that of AuNPs in the visible range. The resonance wavelength of AuNSs shifted to longer wavelengths compared to that of AuNSs dispersed in water/BuOH solution (without AuNPs) used as a reference. This resonance wavelength shift is similar to that observed in the formation of AuNSs (core)/AuNPs (satellite) nanostructures reported in the past [24]. Therefore, this resonance wavelength shift is attributed to the plasmon coupling between AuNSs and AuNPs, suggesting the formation of AuNPs/AuNSs complexes. The LSP resonance of AuNSs was not clearly observed under conditions where the number of AuNSs was low ( $<2.1 \times 10^9$ ); however, the formation of AuNSs/AuNPs complexes is still anticipated. Furthermore, the average hydrodynamic diameter of the colloidal solution immediately after mixing both nanoparticles in water/BuOH was measured by DLS measurements (Figure 1B). Under conditions where the number of AuNSs was low ( $5.3 \times 10^8$  and  $1.1 \times 10^9$ ), the particles exhibited a hydrodynamic diameter similar to that of AuNPs measured as a reference (74 nm) in BuOH. However, as the number of AuNSs in the solution increased, the hydrodynamic diameter also increased, surpassing both the hydrodynamic diameters of AuNPs and AuNSs (166 nm). These results suggest the formation of larger nanoparticles (i.e., AuNSs/AuNPs complexes) in water/BuOH compared to AuNSs alone. When the number of AuNSs was low, it is likely that there was not a significant change in hydrodynamic diameter, as the number of AuNSs/AuNPs complexes was overwhelmingly fewer than the number of AuNPs. From these results, it is suggested that when AuNSs and AuNPs were mixed in water/BuOH, their complexes were formed immediately.

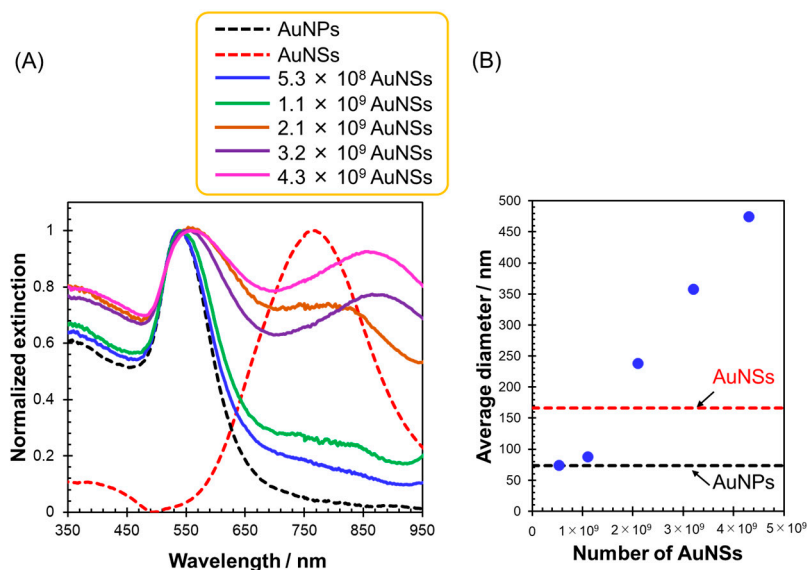


**Figure 1.** Verification of the formation of AuNPs/AuNSs complexes. (A) Extinction spectra of the colloidal solution obtained immediately after mixing AuNPs with AuNSs in water/BuOH. (B) Plots of average hydrodynamic diameter of the colloidal solution estimated by DLS measurements immediately after mixing AuNPs with AuNSs in water/BuOH.

Next, the assembling behavior of these nanoparticles to the air/water interface was investigated. When only AuNSs were dispersed in the water/BuOH solution, there was no assembling of AuNSs to the air/water interface even after 5 h. This is because, as mentioned above, the assembling properties to the air/water interface are only exhibited by the nanoparticles protected with PVP [36]. Therefore, when only PVP-protected AuNPs were dispersed in water/BuOH, the red color attributed to the LSP resonance of AuNPs in

the solution faded with time, and a uniform blue liquid-like film formed at the air/water interface (Figure 2A). This is the result of the spontaneous assembly of AuNPs dispersed in water/BuOH at the air/water interface. Next, the color of the mixed solution of AuNPs and AuNSs is discussed. Under conditions of low AuNS numbers (Figure 2B,C), the solution color immediately after mixing AuNPs with AuNSs was similar to that in Figure 2A. This is supported by the fact that, as shown in Figure 1A, the LSP resonance band of AuNPs remained largely unchanged, while the LSP resonance band of AuNSs is significantly lower compared to that of AuNPs, due to the low number of mixed AuNSs. On the other hand, in Figure 2D–F, the color of the solution faded from red and exhibited a darker blue hue compared to the AuNPs colloidal solution. This corresponds to significant spectral changes in the extinction spectrum (i.e., broadening of the LSP resonance band of AuNPs and enhancement of the LSP resonance band of AuNSs, as shown in Figure 1A), resulting from the increase in the number of AuNSs and the formation of numerous AuNPs/AuNSs complexes. Furthermore, it is worth emphasizing that even when various numbers of AuNSs were mixed with AuNPs in water/BuOH, the solution color faded with time, and the formation of a distinct liquid-like film on the air/water interface was observed (Figure 2B–F). After 90 min, the solution color became almost colorless and transparent for all samples, suggesting that both AuNPs alone and AuNPs/AuNSs complexes accumulated from the solution to the air/water interface. It is worth noting that as the number of AuNSs increased, the color of the film formed at the air/water interface became darker, and the area of the film decreased. Particularly, in samples with AuNS numbers of  $3.2 \times 10^9$  and  $4.3 \times 10^9$ , darker films were observed only at the rim of the dish. The reason for this position-selective accumulation is currently unclear. Furthermore, the extinction spectra of the water/BuOH solutions accompanying the nanoparticle assembly at the air/water interface were measured.

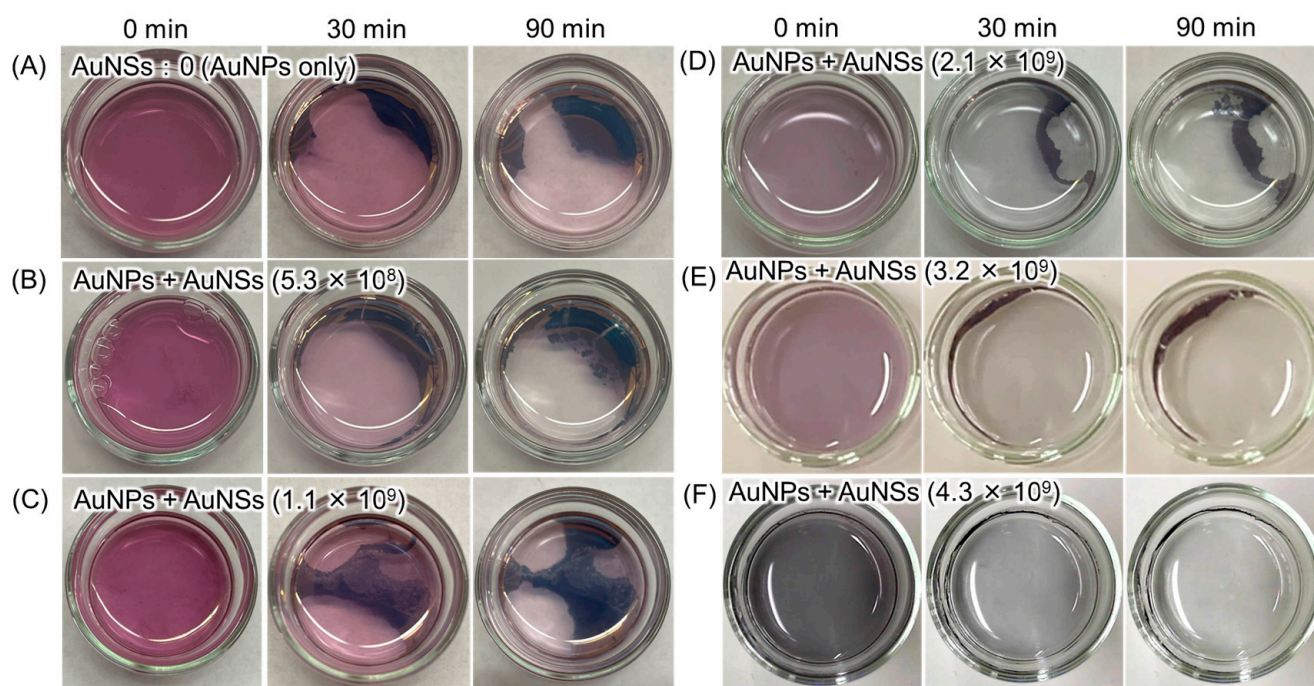


**Figure 2.** Photographs of the assembling process of nanoparticles from water/BuOH to air/water interface. (A) The formation of assemblies from the colloidal solution of AuNPs (quantity:  $5.5 \times 10^{11}$ ) without AuNSs. (B–F) The assemblies formed from solutions where AuNPs (quantity:  $5.5 \times 10^{11}$ ) were mixed with (B)  $5.3 \times 10^8$ , (C)  $1.1 \times 10^9$ , (D)  $2.1 \times 10^9$ , (E)  $3.2 \times 10^9$ , and (F)  $4.3 \times 10^9$  AuNSs, respectively.

The spectrum of the water/BuOH solution containing only dispersed AuNPs, measured for reference (Figure 3A), showed a decrease in the LSP resonance band of AuNPs in the visible range with time. This decrease is attributed to the assembly of AuNPs to

the air/water interface, leading to a decrease in the number of AuNPs in the solution. Additionally, Figure 3B shows the extinction spectrum of a solution where both AuNPs and  $3.2 \times 10^9$  AuNSs are mixed together as a typical example (the extinction spectra for conditions with other numbers of AuNSs are presented in Figure S2). In addition to the decrease in the LSP resonance band of AuNPs with time, the extinction band in the near-infrared region attributed to the LSP resonance band of the AuNPs/AuNSs complexes also decreased similarly to that of AuNPs. These results confirm that AuNSs alone do not accumulate at the air/water interface; however, after forming complexes with AuNPs, they do assemble at the air/water interface. When AuNPs form complexes with AuNSs, it suggests that the capability of AuNPs to accumulate at the air/water interface remains intact even within the complexes.

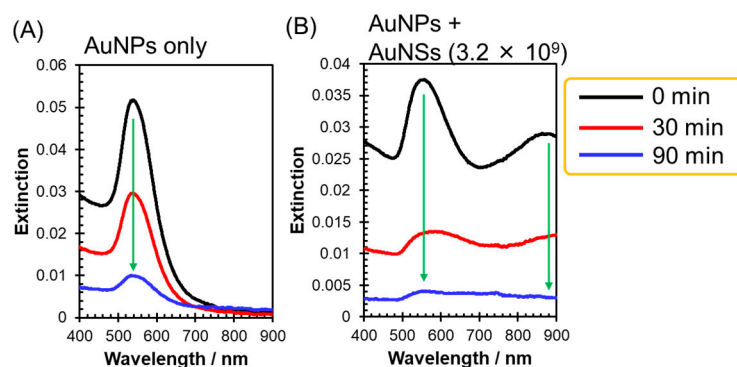


**Figure 3.** Time-dependent extinction spectra of the water/BuOH solution: (A) Only dispersed AuNPs (quantity:  $5.5 \times 10^{11}$ ) and (B) AuNPs (quantity:  $5.5 \times 10^{11}$ ) with AuNSs (quantity:  $3.2 \times 10^9$ ).

Next, the nanoparticle assemblies formed at the air/water interface were transferred onto glass substrates, and their morphology was observed using SEM. As shown in Figure 4A, the assemblies formed solely with AuNPs exhibited high-density two-dimensional structures. On the other hand, when the number of AuNSs was  $5.3 \times 10^8$  and  $1.1 \times 10^9$  (Figure 4B,C), typical AuNP/AuNS-in-assemblies were formed (inset in Figure 4B), with AuNPs/AuNSs complexes sparsely dispersed throughout the AuNP two-dimensional assemblies. When the number of AuNSs was  $>2.1 \times 10^9$ , the two-dimensional assemblies of AuNPs was hardly observed, and only a heterogeneous three-dimensional network structures consisting of AuNPs and AuNSs was observed (Figure 4D–F). This formation is likely attributed to the increase in the number of AuNSs in water/BuOH. Consequently, there is a higher number of AuNPs/AuNSs complexes, which then aggregated randomly at the air/water interface due to strong hydrophobic interactions among these complexes.

The morphology of these nanoparticle assemblies transferred onto glass substrates was also examined using AFM measurements. In the AuNP assemblies composed solely of AuNPs (Figure 5A), the formation of a uniform nanoparticle film, consistent with the SEM observations (Figure 4A), was confirmed. The average film thickness was measured to be  $45 \pm 1.8$  nm, which was consistent with the size of AuNPs estimated from TEM images (Figure S1). These results indicate the formation of a monolayer of AuNPs. For samples with AuNS numbers of  $5.3 \times 10^8$  and  $1.1 \times 10^9$  (Figure 5B,C), larger materials than AuNPs and AuNSs (Figure S3), presumably AuNPs/AuNSs complexes, were observed to be dispersed within the uniform AuNP assemblies. Furthermore, TEM observations (Figure S1C) confirmed that this complex is composed of AuNPs and AuNSs. Additionally, an increase in the number of AuNSs was found to increase the density of AuNPs/AuNSs complexes: when the number of AuNSs was  $5.3 \times 10^8$ , the density of AuNPs/AuNSs complexes was  $12 \pm 3.3/\mu\text{m}^2$ , and when it was  $1.1 \times 10^9$ , the density was  $22 \pm 2.9/\mu\text{m}^2$ . On the other hand, when the number of AuNSs exceeded  $2.1 \times 10^9$ , the formation of a thick ( $>350$  nm) and heterogeneous three-dimensional network structure was observed, consistent with the SEM observations (Figure 5D–F).

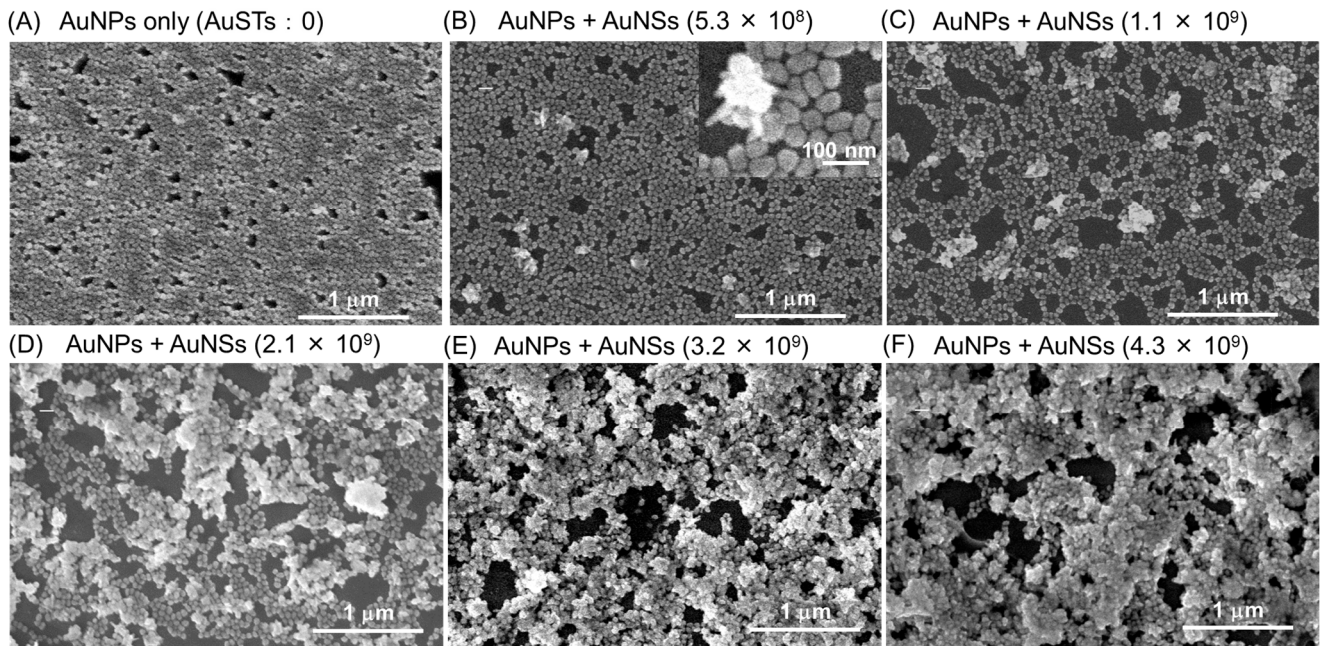


**Figure 4.** SEM images of the assemblies. (A) SEM image of assemblies consisting solely of AuNPs obtained from the colloidal solution of AuNPs (without AuNSs). SEM images of AuNP/AuNS-in-assemblies prepared from solutions where AuNPs (quantity:  $5.5 \times 10^{11}$ ) were mixed with (B)  $5.3 \times 10^8$ , (C)  $1.1 \times 10^9$ , (D)  $2.1 \times 10^9$ , (E)  $3.2 \times 10^9$ , and (F)  $4.3 \times 10^9$  AuNSs.

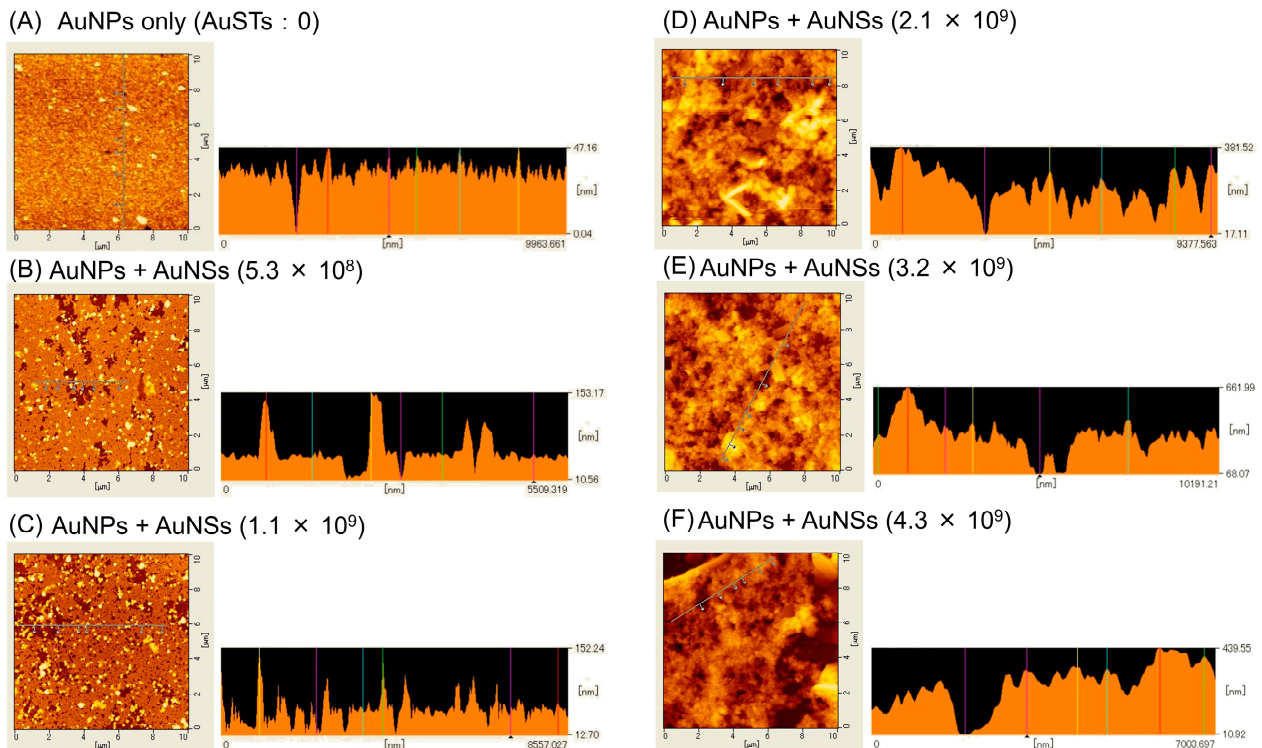


**Figure 5.** AFM images of the assemblies. (A) AFM image of assemblies consisting solely of AuNPs obtained from the colloidal solution of AuNPs (without AuNSs). AFM images of AuNP/AuNS-in-assemblies prepared from solutions where AuNPs (quantity:  $5.5 \times 10^{11}$ ) were mixed with (B)  $5.3 \times 10^8$ , (C)  $1.1 \times 10^9$ , (D)  $2.1 \times 10^9$ , (E)  $3.2 \times 10^9$ , and (F)  $4.3 \times 10^9$  AuNSs.

### 3.2. Optical Properties and SERS Activity of Assemblies

The optical properties of the assemblies produced from water/BuOH containing AuNSs and AuNPs were investigated by measuring their extinction spectra (Figure 6). The assemblies constructed solely with AuNPs as reference samples (i.e., AuNS: 0) exhibited a broad LSP resonance band from 500 to 1000 nm, induced by plasmon coupling between the AuNPs. This optical property was maintained when the number of AuNSs was low ( $5.3 \times 10^8$  and  $1.1 \times 10^9$ ). The assemblies formed under these conditions exhibited optical properties dominated by the assemblies of AuNPs rather than the optical properties of AuNPs/AuNSs complexes, as suggested by the low density of AuNPs/AuNSs complexes, as shown in Figures 4 and 5. On the other hand, under conditions where the number of AuNSs exceeded  $1.1 \times 10^9$ , an increase in the number of AuNSs led to significant broadening of the LSP resonance band. This is attributed to the change in the assembly structure to a random three-dimensional network structure, as can be seen from Figures 4 and 5.

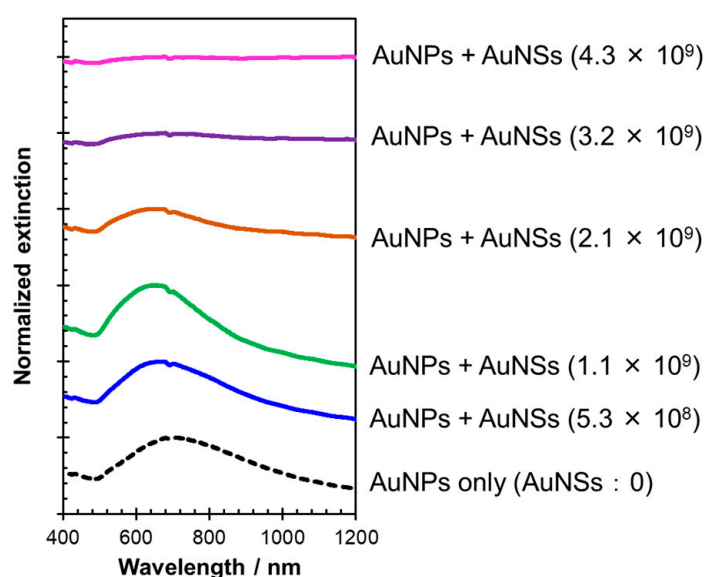


**Figure 6.** Extinction spectra of AuNP/AuNS-in-assemblies on glass plates obtained from a colloidal solution where AuNPs (quantity:  $5.5 \times 10^{11}$ ) were mixed with  $5.3 \times 10^8$ ,  $1.1 \times 10^9$ ,  $2.1 \times 10^9$ ,  $3.2 \times 10^9$ , and  $4.3 \times 10^9$  AuNSs. As a reference, the extinction spectrum of assemblies consisting solely of AuNPs obtained from the colloidal solution of AuNPs (without AuNSs) was also provided.

The SERRS activity of these nanoparticle assemblies was investigated using ICG as a Raman probe. SERRS spectrum patterns derived from ICG were obtained from ICG-modified AuNP/AuNS-in-assemblies, as well as from ICG-modified referenced AuNP two-dimensional assemblies (without AuNSs) (Figure 7A) [32,39,40]. The detailed assignment is described in Figure S4. The SERRS signal from AuNP/AuNS-in-assemblies prepared by mixing with  $5.3 \times 10^8$  and  $1.1 \times 10^9$  AuNSs was significantly higher than that from the reference AuNP assemblies (Figure 7B). Additionally, the signal intensity increased with an increase in the number of AuNSs. However, under conditions where the number of AuNSs corresponding to the formation of three-dimensional random network structures exceeded  $1.1 \times 10^9$ , the SERRS signal intensity remained almost unchanged regardless of the number of AuNSs, similar to AuNP assemblies. These results demonstrate that the two-dimensional assemblies composed of AuNPs and AuNPs/AuNSs complexes serve as high-performance SERS platforms.

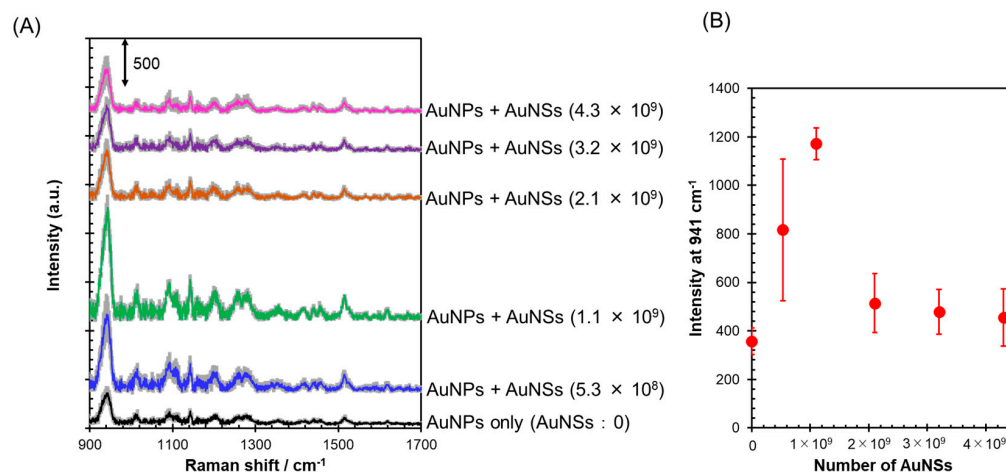


**Figure 7.** SERRS properties of AuNP/AuNS-in-assemblies. **(A)** SERRS spectra of AuNP/AuNS-in-assemblies modified with ICG on glass plates obtained from a colloidal solution where AuNPs (quantity:  $5.5 \times 10^{11}$ ) were mixed with  $5.3 \times 10^8$ ,  $1.1 \times 10^9$ ,  $2.1 \times 10^9$ ,  $3.2 \times 10^9$ , and  $4.3 \times 10^9$  AuNSs. As a reference, SERRS spectrum of assemblies consisting solely of AuNPs obtained from the colloidal solution of AuNPs (without AuNSs) was also provided. **(B)** The intensity of SERRS peak against the number of AuNSs.

We examined the resilience of AuNP/AuNS-in-assemblies, developed in this study for potential application as SERS platforms, against various solvents. The assemblies, transferred onto glass substrates beforehand, were thoroughly washed with toluene, Milli-Q water, and ethanol, yet their optical properties remained unchanged (Figure S5A). Furthermore, from photographs of the assemblies (Figure S5B), it is evident that they remained stable without peeling off during the washing process. Therefore, it can be concluded that the robustness of the assemblies as SERS platforms is high.

#### 4. Conclusions

In this study, we developed a unique structure where hetero AuNPs/AuNSs complexes were dispersed within AuNP two-dimensional assemblies. This was achieved by mixing AuNPs with AuNSs, which interact electrostatically, during the process of preparing AuNP two-dimensional assemblies using Rayleigh–Bénard–Marangoni convection. The SERRS activity of the structure was found to be higher than that of simple AuNP assemblies and correlated with the density of AuNPs/AuNSs complexes. Therefore, it was demonstrated that low-density AuNPs/AuNSs complexes enhanced the SERRS activity of AuNP two-dimensional assemblies. High-density assemblies of plasmonic metal nanoparticles are expected to be applied as SERS platforms enabling the detection of low-concentration biomolecules and pesticide residues for diagnostics and food safety assurance. Therefore, the AuNP/AuNS-in-assemblies have the potential for applications as SERS platforms enabling more sensitive detection of the aforementioned target molecules. In the future, by developing techniques to incorporate further optimized heterocomplexes with nanoparticles of different shapes, sizes, and materials into metal nanoparticle assemblies, a highly sensitive SERS activity platform can be developed. This strategy is currently being pursued in our laboratory.

**Supplementary Materials:** The following supporting information can be downloaded at: <https://www.mdpi.com/article/10.3390/nano14090764/s1>, Figure S1: TEM images of AuNPs and AuNSs. Figure S2: Time-dependent extinction spectra of the water/BuOH solution containing AuNPs and AuNSs. Figure S3: Comparison of morphologies through AFM observations between individual AuNPs and AuNSs, and AuNP/AuNS-in-assemblies. Figure S4: Peak assignments of SERRS spectrum of ICG-modified AuNP/AuNS-in-assemblies. Figure S5: Chemical robustness (stability against solvents) of the AuNP/AuNS-in-assemblies. Ref. [41] is cited in Supplementary Materials.

**Author Contributions:** K.S., J.O. and K.T. initiated and supervised the study. K.O., R.T., Y.H., Y.A. and K.H. carried out the experiments and data analyses. K.S. cowrote the paper. All authors have read and agreed to the published version of the manuscript.

**Funding:** This work was supported by financial aid from JSPS KAKENHI (grant numbers 19H05627 and 23K17961).

**Data Availability Statement:** The data supporting the findings of this study are available in the article and its Supplementary Materials.

**Conflicts of Interest:** The authors state that they have no conflicts of interest or personal relationships that could influence the work reported in this paper.

## References

1. Lenzi, E.; Jimenez de Aberasturi, D.; Liz-Marzán, L.M. Surface-Enhanced Raman Scattering Tags for Three-Dimensional Bioimaging and Biomarker Detection. *ACS Sens.* **2019**, *4*, 1126–1137. [[CrossRef](#)]
2. Hang, Y.; Boryczka, J.; Wu, N. Visible-Light and near-Infrared Fluorescence and Surface-Enhanced Raman Scattering Point-of-Care Sensing and Bio-Imaging: A Review. *Chem. Soc. Rev.* **2022**, *51*, 329–375. [[CrossRef](#)] [[PubMed](#)]
3. Hutter, E.; Fendler, J.H. Exploitation of Localized Surface Plasmon Resonance. *Adv. Mater.* **2004**, *16*, 1685–1706. [[CrossRef](#)]
4. Amendola, V.; Pilot, R.; Frasconi, M.; Maragò, O.M.; Iatì, M.A. Surface Plasmon Resonance in Gold Nanoparticles: A Review. *J. Phys. Condens. Matter* **2017**, *29*, 203002. [[CrossRef](#)] [[PubMed](#)]
5. Kneipp, K.; Kneipp, H.; Itzkan, I.; Dasari, R.R.; Feld, M.S. Surface-Enhanced Raman Scattering and Biophysics. *J. Phys. Condens. Matter* **2002**, *14*, 202. [[CrossRef](#)]
6. Ghosh, S.K.; Pal, T. Interparticle Coupling Effect on the Surface Plasmon Resonance of Gold Nanoparticles: From Theory to Applications. *Chem. Rev.* **2007**, *107*, 4797–4862. [[CrossRef](#)] [[PubMed](#)]
7. Halas, N.J.; Lal, S.; Chang, W.-S.; Link, S.; Nordlander, P. Plasmons in Strongly Coupled Metallic Nanostructures. *Chem. Rev.* **2011**, *111*, 3913–3961. [[CrossRef](#)] [[PubMed](#)]
8. Gwo, S.; Chen, H.-Y.; Lin, M.-H.; Sun, L.; Li, X. Nanomanipulation and Controlled Self-Assembly of Metal Nanoparticles and Nanocrystals for Plasmonics. *Chem. Soc. Rev.* **2016**, *45*, 5672–5716. [[CrossRef](#)] [[PubMed](#)]
9. Lee, H.K.; Lee, Y.H.; Koh, C.S.L.; Phan-Quang, G.C.; Han, X.; Lay, C.L.; Sim, H.Y.F.; Kao, Y.-C.; An, Q.; Ling, X.Y. Designing Surface-Enhanced Raman Scattering (SERS) Platforms beyond Hotspot Engineering: Emerging Opportunities in Analyte Manipulations and Hybrid Materials. *Chem. Soc. Rev.* **2019**, *48*, 731–756. [[CrossRef](#)]
10. Ding, S.-Y.; You, E.-M.; Tian, Z.-Q.; Moskovits, M. Electromagnetic Theories of Surface-Enhanced Raman Spectroscopy. *Chem. Soc. Rev.* **2017**, *46*, 4042–4076. [[CrossRef](#)]
11. Sugawa, K.; Akiyama, T.; Tanoue, Y.; Harumoto, T.; Yanagida, S.; Yasumori, A.; Tomita, S.; Otsuki, J. Particle Size Dependence of the Surface-Enhanced Raman Scattering Properties of Densely Arranged Two-Dimensional Assemblies of Au(Core)–Ag(Shell) Nanospheres. *Phys. Chem. Chem. Phys.* **2015**, *17*, 21182–21189. [[CrossRef](#)] [[PubMed](#)]
12. Tanoue, Y.; Sugawa, K.; Yamamuro, T.; Akiyama, T. Densely Arranged Two-Dimensional Silver Nanoparticle Assemblies with Optical Uniformity over Vast Areas as Excellent Surface-Enhanced Raman Scattering Substrates. *Phys. Chem. Chem. Phys.* **2013**, *15*, 15802–15805. [[CrossRef](#)] [[PubMed](#)]
13. Kim, M.; Kwon, H.; Lee, S.; Yoon, S. Effect of Nanogap Morphology on Plasmon Coupling. *ACS Nano* **2019**, *13*, 12100–12108. [[CrossRef](#)] [[PubMed](#)]
14. Tian, Y.; Shuai, Z.; Shen, J.; Zhang, L.; Chen, S.; Song, C.; Zhao, B.; Fan, Q.; Wang, L. Plasmonic Heterodimers with Binding Site-Dependent Hot Spot for Surface-Enhanced Raman Scattering. *Small* **2018**, *14*, 1800669. [[CrossRef](#)] [[PubMed](#)]
15. Höller, R.P.M.; Kuttner, C.; Mayer, M.; Wang, R.; Dulle, M.; Contreras-Cáceres, R.; Fery, A.; Liz-Marzán, L.M. Colloidal Superstructures with Triangular Cores: Size Effects on SERS Efficiency. *ACS Photonics* **2020**, *7*, 1839–1848. [[CrossRef](#)]
16. Popp, P.S.; Herrmann, J.F.; Fritz, E.-C.; Ravoo, B.J.; Höppener, C. Impact of the Nanoscale Gap Morphology on the Plasmon Coupling in Asymmetric Nanoparticle Dimer Antennas. *Small* **2016**, *12*, 1667–1675. [[CrossRef](#)] [[PubMed](#)]
17. Rong, Z.; Xiao, R.; Wang, C.; Wang, D.; Wang, S. Plasmonic Ag Core–Satellite Nanostructures with a Tunable Silica-Spaced Nanogap for Surface-Enhanced Raman Scattering. *Langmuir* **2015**, *31*, 8129–8137. [[CrossRef](#)] [[PubMed](#)]
18. Ávalos-Ovando, O.; Besteiro, L.V.; Wang, Z.; Govorov, A.O. Temporal Plasmonics: Fano and Rabi Regimes in the Time Domain in Metal Nanostructures. *Nanophotonics* **2020**, *9*, 3587–3595. [[CrossRef](#)]
19. Bachelier, G.; Russier-Antoine, I.; Benichou, E.; Jonin, C.; Del Fatti, N.; Vallée, F.; Brevet, P.-F. Fano Profiles Induced by Near-Field Coupling in Heterogeneous Dimers of Gold and Silver Nanoparticles. *Phys. Rev. Lett.* **2008**, *101*, 197401. [[CrossRef](#)]
20. Sheikholeslami, S.; Jun, Y.; Jain, P.K.; Alivisatos, A.P. Coupling of Optical Resonances in a Compositionally Asymmetric Plasmonic Nanoparticle Dimer. *Nano Lett.* **2010**, *10*, 2655–2660. [[CrossRef](#)]
21. Lee, D.; Yoon, S. Gold Nanocube–Nanosphere Dimers: Preparation, Plasmon Coupling, and Surface-Enhanced Raman Scattering. *J. Phys. Chem. C* **2015**, *119*, 7873–7882. [[CrossRef](#)]

22. Becerril-Castro, I.B.; Calderon, I.; Pazos-Perez, N.; Guerrini, L.; Schulz, F.; Feliu, N.; Chakraborty, I.; Giannini, V.; Parak, W.J.; Alvarez-Puebla, R.A. Gold Nanostars: Synthesis, Optical and SERS Analytical Properties. *Anal. Sens.* **2022**, *2*, e202200005. [[CrossRef](#)]
23. Tsoulos, T.V.; Fabris, L. Interface and Bulk Standing Waves Drive the Coupling of Plasmonic Nanostar Antennas. *J. Phys. Chem. C* **2018**, *122*, 28949–28957. [[CrossRef](#)]
24. Indrasekara, A.S.D.S.; Thomas, R.; Fabris, L. Plasmonic Properties of Regiospecific Core–Satellite Assemblies of Gold Nanostars and Nanospheres. *Phys. Chem. Chem. Phys.* **2015**, *17*, 21133–21142. [[CrossRef](#)] [[PubMed](#)]
25. Ellis, M.G.; Pant, U.; Lou-Franco, J.; Logan, N.; Cao, C. Directed Assembly of Au Nanostar@Ag Satellite Nanostructures for SERS-Based Sensing of Hg<sup>2+</sup> Ions. *ACS Appl. Nano Mater.* **2023**, *6*, 10431–10440. [[CrossRef](#)]
26. Trinh, H.D.; Kim, S.; Yun, S.; Huynh, L.T.M.; Yoon, S. Combinatorial Approach to Find Nanoparticle Assemblies with Maximum Surface-Enhanced Raman Scattering. *ACS Appl. Mater. Interfaces* **2024**, *16*, 1805–1814. [[CrossRef](#)] [[PubMed](#)]
27. Lee, Y.H.; Shi, W.; Lee, H.K.; Jiang, R.; Phang, I.Y.; Cui, Y.; Isa, L.; Yang, Y.; Wang, J.; Li, S.; et al. Nanoscale Surface Chemistry Directs the Tunable Assembly of Silver Octahedra into Three Two-Dimensional Plasmonic Superlattices. *Nat. Commun.* **2015**, *6*, 6990. [[CrossRef](#)]
28. Lin, S.; Lin, X.; Shang, Y.; Han, S.; Hasi, W.; Wang, L. Self-Assembly of Faceted Gold Nanocrystals for Surface-Enhanced Raman Scattering Application. *J. Phys. Chem. C* **2019**, *123*, 24714–24722. [[CrossRef](#)]
29. Yang, G.; Nanda, J.; Wang, B.; Chen, G.; Hallinan, D.T. Self-Assembly of Large Gold Nanoparticles for Surface-Enhanced Raman Spectroscopy. *ACS Appl. Mater. Interfaces* **2017**, *9*, 13457–13470. [[CrossRef](#)]
30. Lin, S.; Guan, H.; Liu, Y.; Huang, S.; Li, J.; Hasi, W.; Xu, Y.; Zou, J.; Dong, B. Binary Plasmonic Assembly Films with Hotspot-Type-Dependent Surface-Enhanced Raman Scattering Properties. *ACS Appl. Mater. Interfaces* **2021**, *13*, 53289–53299. [[CrossRef](#)]
31. Shi, Q.; Sikdar, D.; Fu, R.; Si, K.J.; Dong, D.; Liu, Y.; Premaratne, M.; Cheng, W. 2D Binary Plasmonic Nanoassemblies with Semiconductor n/P-Doping-Like Properties. *Adv. Mater.* **2018**, *30*, 1801118. [[CrossRef](#)] [[PubMed](#)]
32. Wang, H.; Levin, C.S.; Halas, N.J. Nanosphere Arrays with Controlled Sub-10-Nm Gaps as Surface-Enhanced Raman Spectroscopy Substrates. *J. Am. Chem. Soc.* **2005**, *127*, 14992–14993. [[CrossRef](#)] [[PubMed](#)]
33. Bigioni, T.P.; Lin, X.-M.; Nguyen, T.T.; Corwin, E.I.; Witten, T.A.; Jaeger, H.M. Kinetically Driven Self Assembly of Highly Ordered Nanoparticle Monolayers. *Nat. Mater.* **2006**, *5*, 265–270. [[CrossRef](#)] [[PubMed](#)]
34. Xu, Y.; Konrad, M.P.; Lee, W.W.Y.; Ye, Z.; Bell, S.E.J. A Method for Promoting Assembly of Metallic and Nonmetallic Nanoparticles into Interfacial Monolayer Films. *Nano Lett.* **2016**, *16*, 5255–5260. [[CrossRef](#)] [[PubMed](#)]
35. Duan, H.; Wang, D.; Kurth, D.G.; Möhwald, H. Directing Self-Assembly of Nanoparticles at Water/Oil Interfaces. *Angew. Chem. Int. Ed.* **2004**, *43*, 5639–5642. [[CrossRef](#)]
36. Sugawa, K.; Hayakawa, Y.; Aida, Y.; Kajino, Y.; Tamada, K. Two-Dimensional Assembled PVP-Modified Silver Nanoprisms Guided by Butanol for Surface-Enhanced Raman Scattering-Based Invisible Printing Platforms. *Nanoscale* **2022**, *14*, 9278–9285. [[CrossRef](#)] [[PubMed](#)]
37. Turkevich, J.; Stevenson, P.C.; Hillier, J. A Study of the Nucleation and Growth Processes in the Synthesis of Colloidal Gold. *Discuss. Faraday Soc.* **1951**, *11*, 55. [[CrossRef](#)]
38. Yuan, H.; Fales, A.M.; Vo-Dinh, T. TAT Peptide-Functionalized Gold Nanostars: Enhanced Intracellular Delivery and Efficient NIR Photothermal Therapy Using Ultralow Irradiance. *J. Am. Chem. Soc.* **2012**, *134*, 11358–11361. [[CrossRef](#)] [[PubMed](#)]
39. Kneipp, J.; Kneipp, H.; Rice, W.L.; Kneipp, K. Optical Probes for Biological Applications Based on Surface-Enhanced Raman Scattering from Indocyanine Green on Gold Nanoparticles. *Anal. Chem.* **2005**, *77*, 2381–2385. [[CrossRef](#)]
40. Guerrini, L.; Jurasekova, Z.; del Puerto, E.; Hartsuiker, L.; Domingo, C.; Garcia-Ramos, J.V.; Otto, C.; Sanchez-Cortes, S. Effect of Metal–Liquid Interface Composition on the Adsorption of a Cyanine Dye onto Gold Nanoparticles. *Langmuir* **2013**, *29*, 1139–1147. [[CrossRef](#)]
41. Sugawa, K.; Takeshima, N.; Uchida, K.; Tahara, H.; Jin, S.; Tsunenari, N.; Akiyama, T.; Kusaka, Y.; Fukuda, N.; Ushijima, H.; et al. Photocurrent enhancement of porphyrin molecules over a wide-wavelength region based on combined use of silver nanoprisms with different aspect ratios. *J. Mater. Chem. C* **2015**, *3*, 11439–11448. [[CrossRef](#)]

**Disclaimer/Publisher’s Note:** The statements, opinions and data contained in all publications are solely those of the individual author(s) and contributor(s) and not of MDPI and/or the editor(s). MDPI and/or the editor(s) disclaim responsibility for any injury to people or property resulting from any ideas, methods, instructions or products referred to in the content.